Eur. Phys. J. A (2015) **51**: 169
DOI 10.1140/epja/i2015-15169-9

THE EUROPEAN PHYSICAL JOURNAL A

Review

Uncertainty quantification and propagation in nuclear density functional theory*

N. Schunck[1,a], J.D. McDonnell[1,2], D. Higdon[3], J. Sarich[4], and S.M. Wild[4]

[1] Nuclear and Chemical Science Division, Lawrence Livermore National Laboratory, Livermore, CA 94551, USA
[2] Department of Physics and Astronomy, Francis Marion University, Florence, SC 29501, USA
[3] Los Alamos National Laboratory, Los Alamos, NM 87545, USA
[4] Mathematics and Computer Science Division, Argonne National Laboratory, Argonne, IL 60439, USA

Received: 17 March 2015 / Revised: 30 March 2015
Published online: 23 December 2015 – © Società Italiana di Fisica / Springer-Verlag 2015
Communicated by N. Alamanos

Abstract. Nuclear density functional theory (DFT) is one of the main theoretical tools used to study the properties of heavy and superheavy elements, or to describe the structure of nuclei far from stability. While on-going efforts seek to better root nuclear DFT in the theory of nuclear forces (see Duguet *et al.*, this Topical Issue), energy functionals remain semi-phenomenological constructions that depend on a set of parameters adjusted to experimental data in finite nuclei. In this paper, we review recent efforts to quantify the related uncertainties, and propagate them to model predictions. In particular, we cover the topics of parameter estimation for inverse problems, statistical analysis of model uncertainties and Bayesian inference methods. Illustrative examples are taken from the literature.

1 Introduction

Applications of nuclear science in energy production or national security are based on nuclear data such as cross-sections, energy levels, and lifetimes. In many cases of interest, experimental measurements are not available, and guidance from theory is indispensable. In the valley of stability, one still can employ simple models heavily tuned to existing data. For example, the fission model implemented in the GEF code uses about 50 parameters such as fission barrier heights and level density parameter which are parameterized as a function of Z, N, or neutron incident energy. The code also uses databases of binding energies and shell corrections (in the ground state only). Based on these parameters and data banks, qualitative arguments, and a Monte Carlo sampling scheme, observables such as fission probabilities, fission fragment yields, and neutron multiplicities can be reproduced accurately in the actinide region (with a few exceptions) [1]. While such an empirical approach fulfills some of the needs of data evaluators, however, its predictive power beyond the region where the model is fitted is null. Indeed, such models do not contain any physics principle related to nucleons, their interaction, and the quantum nature of the atomic nucleus.

Therefore, even if data-driven empirical models will always be helpful in the short term, one must try to root data evaluation into more microscopic theories of nuclear structure and reactions in order to gain confidence in the reliability of evaluations. In heavy elements, density functional theory is currently the only candidate for such a microscopic approach to nuclear structure. In particular, recent advances in high-performance computing have enabled large-scale calculations of nuclear properties at the scale of the mass table [2,3]. Despite this progress, however, the accuracy and precision needed in data evaluations represent a formidable challenge for nuclear density functional theory (DFT). As an example, nuclear binding energies are computed within approximately 500 keV in state-of-the-art DFT calculations [4,5]. Although this represents a relative error of 0.05% or less for nuclei with mass $A > 100$, it remains far from the sub-keV accuracy that is demanded in, for example, criticality studies. In order to make data evaluations based on microscopic inputs from DFT a viable alternative to simpler models, two challenges must be addressed in the next few years.

First, DFT must be more firmly and rigorously connected to the theory of nuclear forces as defined, for example, by effective field theory [6]. One possibility is to formally derive local energy functionals from chiral effective field potentials by using the density matrix expansion, and subsequently readjust coupling constants to reproduce properties of finite nuclei [7,8]. Another is to use, for example, many-body perturbation theory to expand

* Contribution to the Topical Issue "Perspectives on Nuclear Data for the Next Decade" edited by Nicolas Alamanos, Eric Bauge, Stéphane Hilaire.

[a] e-mail: schunck1@llnl.gov

energy and norm kernels of ab initio approaches in a form amenable to DFT treatment [9]; see also Duguet *et al.* in this Topical Issue.

Second, irrespective of its mathematical form and physical origin, DFT kernels will always contain a phenomenological component in the sense that they depend on a small set of parameters that must be adjusted to data. In addition to making the theory usable, adjusting these parameters will effectively provide an ad hoc mechanism to capture missing correlations. However, this optimization will induce an obvious dependence on the data and the optimization process itself, in addition to the pre-existing uncertainties related to the form of the functional and possible truncation errors in the numerical implementation. Therefore, rigorous methodology is essential in order to identify, quantify and propagate model uncertainties.

In this paper, we review the progress made in this area over the past 10 years. In sect. 2, we recall the essential aspects of nuclear density functional theory; in particular we discuss the distinction between the self-consistent mean-field theory and the energy density functional (EDF) approach. In sect. 3, we look at DFT from a statistician's point of view: What are the parameters of the model? How can they be determined? How can we quantify the statistical uncertainties? We summarize the various tools used to answer these questions. In sect. 4, we review the most recent attempts to propagate statistical uncertainties in model predictions using either covariance techniques or Bayesian inference.

2 Nuclear density functional theory

Density functional theory is a general approach for solving the quantum many-body problem. Its most rigorous formulation is in electronic structure theory, where it is based on the existence theorem of Hohenberg and Kohn [10]. It states that the energy of an interacting electron gas can be written as a functional of the one-body local density (of electrons), and the minimum of this functional gives the exact ground state of the system. Shortly thereafter, this formal existence theorem was supplemented with the Kohn-Sham scheme, which allows one to determine the actual density of electrons that minimizes the energy (if the functional itself is known) by solving equations analogous to Hartree equations [11]. Various extensions have been proposed to handle exchange energy exactly (the Kohn-Sham equations then are similar to Hartree-Fock equations), excited states, systems at finite temperature, and superfluid correlations (see, *e.g.*, [12, 13]). These extensions rely on reformulating the Kohn-Sham scheme with the full one-body density matrix (rather than the local density), density operators, a combination of one- and two-body densities, and so forth. Other extensions account for relativistic effects [14].

Implementations of DFT in nuclear physics are less straightforward, since the nuclear Hamiltonian is not known, in contrast with electronic structure theory. In addition, nuclei are self-bound, and correlation effects are much stronger than in electron systems [6]. Consequently, most nuclear energy functionals used so far have been in fact derived from the expectation value on the quasiparticle vacuum of effective nuclear forces used in the self-consistent nuclear mean-field theory [15]. Therefore, they are formulated in terms of the intrinsic one-body nonlocal density matrix and nonlocal pairing tensor, which can break symmetries of realistic nuclear forces such as translational or rotational invariance, parity, time-reversal invariance, and particle number. This spontaneous symmetry breaking is essential for introducing long-range correlations in the nuclear wave function [16, 17]. Nuclear energy functionals are, therefore, substantially different from their counterpart in electronic DFT. This difference is reflected in the name of energy density functional (EDF) formalism.

2.1 The energy density functional approach

In this section, we succinctly describe the basic ingredients of the single-reference EDF (SR-EDF) approach with non-relativistic empirical functionals such as derived from the Skyrme or Gogny effective interactions. We refer to [6,17] for discussions of more general frameworks such as multireference EDF and ab initio DFT. The starting point is a set of single-particle states $|i\rangle$ that form a basis of the one-body Hilbert space. The related creation/annihilation operators are $c_i^\dagger$ and c_i and define the configuration space representation of the Fock space [16, 18]. The coordinate space representation is obtained by invoking the continuous basis $|x\rangle \equiv |\boldsymbol{r}\sigma\tau\rangle$ of the one-body Hilbert space, with $\sigma = \pm 1/2$ the intrinsic spin projection and $\tau = \pm 1/2$ the isospin projection. The single-particle functions are then $\langle x|i\rangle = \phi_i(x)$, and the corresponding creation/annihilation operators are the field operators $c^\dagger(x)$ and $c(x)$. The particle vacuum of the Fock space is denoted by $|0\rangle$ and is characterized by the property that $\forall\, i, c_i|0\rangle = 0$, or, alternatively, $\forall\, x, c(x)|0\rangle = 0$.

Because of the importance of pairing correlations in low-energy nuclear structure [19], we introduce a canonical transformation between particle operators and quasiparticle operators $\beta_\mu, \beta_\mu^\dagger$. This Bogoliubov-Valatin transformation is characterized by the matrices U and V [15,18,20,21]

$$\begin{aligned}\beta_\mu &= \sum_m \left[U_{\mu m}^\dagger\, c_m + V_{\mu m}^\dagger\, c_m^\dagger\right],\\ \beta_\mu^\dagger &= \sum_m \left[V_{\mu m}^T\, c_m + U_{\mu m}^T\, c_m^\dagger\right].\end{aligned} \tag{1}$$

In the SR-EDF approach, we introduce the reference state $|\Phi\rangle$ as a product wave function of quasiparticle operators acting on the particle vacuum,

$$|\Phi\rangle = \prod_\mu \beta_\mu|0\rangle. \tag{2}$$

Note that, by construction, the quasiparticle vacuum (2) does not conserve particle number.

The next step is to recall that for any given many-body state $|\Psi\rangle$, the one-body density matrix ρ and two-body

pairing tensor κ are defined in configuration space as

$$\rho_{ij} = \frac{\langle\Psi|c_j^\dagger c_i|\Psi\rangle}{\langle\Psi|\Psi\rangle}\,, \qquad \kappa_{ij} = \frac{\langle\Psi|c_j c_i|\Psi\rangle}{\langle\Psi|\Psi\rangle}\,, \tag{3}$$

and the generalized density $\mathcal{R}$ as

$$\mathcal{R} = \begin{pmatrix} \rho & \kappa \\ -\kappa^* & 1-\rho^* \end{pmatrix}. \tag{4}$$

When $|\Psi\rangle$ is the quasiparticle vacuum (2), the corresponding generalized density matrix verifies $\mathcal{R}^2 = \mathcal{R}$ and $\mathcal{R}^\dagger = \mathcal{R}$ [18]. In addition, the Wick theorem ensures that the expectation values of any operator on the quasiparticle vacuum can be expressed as functions of ρ, κ and κ^* alone. These three mathematical objects are thus the basic degrees of freedom of the theory. In particular, the energy is then expressed as a functional $E[\rho, \kappa, \kappa^*]$.

The actual density and pairing tensor of the nucleus in its ground state are determined by solving the Hartree-Fock-Bogoliubov (HFB) equations, which are obtained by applying the variational principle with respect to ρ, κ, and κ^* [15,16,18]. This leads to

$$[\mathcal{H}, \mathcal{R}] = 0, \tag{5}$$

where $\mathcal{H}$ is the HFB matrix, $\mathcal{H}_{ij} = \partial E/\partial \mathcal{R}_{ji}$. One-body observables can then be computed as the trace of the relevant operator and ρ. Because of the nonlinear nature of the HFB equations, it is possible for the generalized density to break various symmetries of nuclear forces. Conversely, conserved symmetries can be used to label quasiparticle states [22–24]. In practice, the HFB equations (5) are solved iteratively. The most common approach is to adopt the following iterative procedure:

1) Choose an initial guess for the density matrix $\rho^{(n)}$ and pairing tensor $\kappa^{(n)}$ (hence the generalized density matrix $\mathcal{R}^{(n)}$) at the first iteration, $n = 1$.
2) Build the HFB matrix from $\mathcal{H}^{(n)} = \partial E/\partial \mathcal{R}^{(n)}$ at the first iteration, $n = 1$.
3) Diagonalize $\mathcal{H}^{(n)}$: this provides the matrices U and V of the Bogoliubov transformation at the first iteration, $n = 1$.
4) These matrices can be used to compute the density matrix and pairing tensor at the next iteration $n = 2$ according to $\rho^{(n+1)} = V^* V^T$ and $\kappa^{(n+1)} = V^* U^T$.
5) Go back to step 1 and repeat until the densities do not change. In practice, this can be decided by imposing that the maximum value of the matrix $|\rho_{ij}|$ does not exceed some criterion ε.

Various techniques can be employed to try and reduce the number of iterations [25]. Another popular approach to solving the HFB equations is the generalized gradient method: it is an iterative procedure that does not rely on successive matrix diagonalizations [16].

2.2 Pseudopotentials and energy functionals

Until recently, most applications of the nuclear EDF approach have been based on semi-empirical EDFs explicitly derived from the expectation value of effective two-body forces $\hat{V}_{\text{eff.}}$ on the quasiparticle vacuum,

$$E[\rho, \kappa, \kappa^*] = \frac{\langle\Phi|\hat{T} + \hat{V}_{\text{eff.}}|\Phi\rangle}{\langle\Phi|\Phi\rangle}\,, \tag{6}$$

where $\hat{T}$ is the kinetic energy operator. In particular, the Skyrme effective force is a zero-range two-body pseudopotential for which the EDF becomes a functional of the local density only [26,27]. The Gogny force has a finite range and gives a functional of the nonlocal one-body density [28]; see, for example, [15,29] for comprehensive reviews of applications of Skyrme and Gogny EDFs. The empirical nature of both the Skyrme and Gogny potentials is manifested by the presence of density dependencies, which prohibits writing the potential in strict second quantization form [30]. With the exception of a few recent applications [31–33], these EDFs have been used in the context of the self-consistent mean-field theory rather than in a strict Kohn-Sham scheme.

In particular, many applications used the underlying effective pseudopotential $\hat{V}_{\text{eff.}}$ to implement beyond mean-field techniques, where EDF reference states of the type (2) serve as basis states to expand the unknown many-body wave function, for example, in the generator coordinate method, or to restore broken symmetries by using projection techniques [15,16]. A few years ago, however, standard beyond mean-field techniques were shown to be invalid with density-dependent pseudopotentials [34–38]. This result has stimulated efforts to remove density dependencies, for example by using momentum-dependent two-body pseudopotentials [39] or zero-range two- and three-body pseudopotentials [40,41]. Since these pseudopotentials are specifically designed to enable beyond mean-field techniques such as projection and configuration mixing, the central element of all these approaches is the effective Hamiltonian $\hat{T} + \hat{V}_{\text{eff.}}$ rather than the EDF itself.

An alternative route is to implement a strict Kohn-Sham approach, where the only degrees of freedom are ρ, κ, and κ^*, the ground-state wave function is always a quasiparticle vacuum of the form (2), and there is no mention of some underlying effective potential $\hat{V}_{\text{eff.}}$. In such an approach, the energy functional $E[\rho, \kappa, \kappa^*]$ must be designed so that it contains all relevant types of correlations. Only two main families of such functionals have been proposed in the literature: those proposed by Fayans and Collaborators [42–44], and the BPCM functionals from the Barcelona-Paris-Cataña-Madrid Collaboration [45,46]. The main difficulty of this strict Kohn-Sham scheme, which is more in line with the spirit of DFT as encountered in electronic structure theory, is to incorporate beyond mean-field correlations accounting, for example, for large amplitude collective motion, or symmetry restoration. Recent work suggests that this could be achieved by introducing new densities representing collective degrees of freedom such as two-body or "collective" densities [47–50] (which may lead to a generalization of the Kohn-Sham equations) or by adding specific terms to the functional designed to cancel symmetry breaking [51,52].

2.3 Pairing correlations

Sometimes overlooked is the fact that, according to the Hohenberg-Kohn theorem, the exact ground state of the system can in principle be expressed entirely as a functional of the local one-body density matrix only. If this theorem could be extended directly to nuclear functionals of the intrinsic one-body density (see, *e.g.*, [53, 54]), pairing correlations could —in principle— be produced by an unique functional of $\rho(\boldsymbol{r})$. In this idealized scenario, there would be no need for quasiparticle operators, the Bogoliubov transformation, or the pairing tensor: the Kohn-Sham scheme would be implemented directly with EDF reference states taken as particle-number-conserving Slater determinants.

In practice, of course, the form of this functional is totally unknown. Until further notice, therefore, it seems more reasonable to build on the success of the self-consistent mean-field theory, to seek an explicit pairing term that is a functional of the usual pairing tensor, and to work with symmetry-breaking reference states as in eq. (2). Recall that the pairing tensor is defined from the specific form that the two-body correlation function takes in an HFB vacuum [12,47]. If we denote $\rho_2(x_1, x_2, x_1', x_2')$ as the full, nonlocal, two-body density matrix, then we have

$$\begin{aligned}\rho_2(x_1, x_2, x_1', x_2') = \kappa^*(x_1, x_2)\kappa(x_2', x_1') \\ -\rho(x_2', x_1)\rho(x_1', x_2) \\ +\rho(x_1', x_1)\rho(x_2', x_2).\end{aligned} \tag{7}$$

Because of this property, the pairing tensor κ and its complex conjugate κ^* are, indeed, the two only degrees of freedom needed to account for pairing correlations at the HFB level.

The pairing EDF can then be obtained by taking the expectation value of a pseudopotential $\hat{V}_{\text{eff.}}^{(\text{pair})}$ on the quasiparticle vacuum, which will immediately introduce a dependence on κ^* and κ. This potential can be the same as the one used in the particle-hole channel, which is typically the choice retained when working with the Gogny force [28]. It can also have a different form, ranging from simple seniority pairing forces [16] to density-dependent zero-range pairing forces [55] to separable expansion of finite-range, Gogny-like potentials [56, 57]. Most of these pairing forces, and hence the resulting pairing functionals, are characterized by only a few parameters, and all lead to EDFs that are functionals of κ^* and κ only.

3 Density functional theory as a model

Whether building the description of atomic nuclei on an effective potential $\hat{V}_{\text{eff.}}$ that defines both the mean-field and beyond mean-field corrections, or an EDF $E[\rho, \kappa, \kappa^*]$ in a strict Kohn-Sham framework, theoretical predictions will depend on a set of unknown parameters $\boldsymbol{x}$ corresponding, respectively, to the parameters of the effective nuclear force or the coupling constants of the EDF. Some of these parameters may be constrained by exploring the connections with the theory of realistic nuclear forces or investigating ideal systems such as nuclear matter or neutron drops [58, 59]. In general, however, one will also have to introduce experimental data in nuclei in order to set the values of these parameters. This fit of low-energy coupling constants to experimental data belongs to the class of inverse problems in statistics. In this section, we review some of the techniques used in nuclear DFT to solve this problem. Most of our considerations are based on the SR-EDF approach to nuclear structure but are easily extended to the self-consistent mean-field approach.

3.1 Parameter estimation

The problem of determining the parameters of the nuclear EDF is easily posed: one needs only to choose a set of data points, define an objective function such as a χ^2 function, and minimize the objective function with respect to the parameters. We use the following notations: $\boldsymbol{y}$ denotes the values of a set of experimental observables, with y_{ti} the value of the i-th observable of type t; $\boldsymbol{x} \equiv (x_1, \ldots, x_{n_x})$ represent the vector of the n_x parameters of the model, that is, the EDF coupling constants in our case; and $\boldsymbol{\eta}$ collects the output of all model calculations. In our case, $\eta_{ti}(\boldsymbol{x})$ is thus the output of an HFB calculation for the ith observable of type t. Also, $\boldsymbol{\epsilon}$ is the vector containing the error between the actual calculation and the experimental value. By definition, we thus have

$$y_{ti} = \eta_{ti}(\boldsymbol{x}) + \epsilon_{ti}, \qquad \epsilon_{ti} \overset{\text{indep}}{\sim} N(0, \sigma_t), \quad \forall\,(t, i). \tag{8}$$

In this expression, $N(0, \sigma_t)$ refers to the normal distribution with mean σ_t. Based on these notations, we minimize the weighted mean squared deviation given by

$$\chi^2(\boldsymbol{x}) = \frac{1}{n_d - n_x} \sum_{t=1}^{T} \sum_{i=1}^{n_t} \left(\frac{y_{ti} - \eta_{ti}(\boldsymbol{x})}{\sigma_t} \right)^2, \tag{9}$$

where T is the total number of different data types, n_t the total number of points of type t, and n_d the total number of experimental points, $n_d = \sum_{t=1}^{T} n_t$. By convention, the vector of parameters at the minimum of the χ^2 is noted $\hat{\boldsymbol{x}}$. Recall that $\chi^2 \gg 1$ implies a poor fit, whereas $\chi^2 \approx 1$ indicates a good fit. This is the familiar "χ^2 per degree of freedom". If all errors ϵ_{ti} are independent and normally distributed with mean 0, then the minimization of (9) is equivalent to maximizing the likelihood function [60, 61]. In addition, the χ^2 is a random variable that follows a genuine χ^2 probability distribution function.

3.1.1 Experimental dataset and bias estimation

Choosing which and how many data points to include in the χ^2 is the first important decision, and several strategies have been followed. In nuclear mass models based either on the Skyrme or Gogny force, all available experimental information on atomic masses is used; see [4,5] and

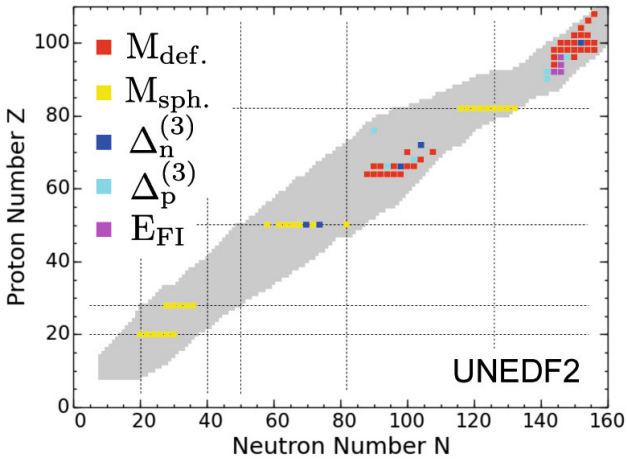

Fig. 1. Experimental data set used for optimizing the UNEDF2 Skyrme functional [33]. For reference, the gray area represents all nuclei where the binding energy is known (based on the 2003 evaluation [66]). Colored squares indicate the nuclei included in the fit of UNEDF2 with the color denoting the type of data: $M_{\mathrm{def.}}$ refer to the binding energy of nuclei that are deformed in their ground-state; $M_{\mathrm{sph.}}$ the binding energy of closed shell nuclei, which are spherical in their ground-state; $\Delta_{\mathrm{n}}^{(3)}$ and $\Delta_{\mathrm{p}}^{(3)}$ refer to the 3-point indicator for the odd-even mass difference for neutrons and protons, respectively; see [67] for a discussion; E_{FI} refers to the excitation energy of the fission isomer; see supplementary material of [33] for the full list of data points.

references therein. It is supplemented by additional data on, for example, fission barriers [62] or neutron matter [4]. The main concern for mass models is the risk of producing a high-bias estimator of the data. In simpler terms, it is by no means guaranteed that mass model parameterizations of Skyrme of Gogny forces are reliable for computing observables that are not masses.

By contrast, most historical fits of the Skyrme and Gogny forces were based on the smallest possible set of data. These included nuclear matter properties, binding energies, radii, and single-particle states; see [15, 29, 63] for a discussion. In addition, data in finite nuclei were taken almost exclusively in doubly magic spherical nuclei: symmetry breaking effects were rarely probed during the optimization itself. Two of the most notable exceptions are the SkM* parameterization of the Skyrme force [64] and the D1S parameterization of the Gogny force [65], which included information on the fission barrier in ^{240}Pu. The combination of small data set and a lack of constraints on nuclear deformation properties is also likely to lead to high-bias estimators.

The recently proposed parameterizations of the Skyrme EDF by the Universal Nuclear Energy Density Functional (UNEDF) Collaboration [3] represent an attempt to reduce the bias of the fitting procedure by taking a medium-sized sample of 100+ data points carefully selected from both spherical and deformed nuclei; see fig. 1 for the specific case of the UNEDF2 functional [31–33]. As a result, the ability of UNEDF functionals to reproduce masses or fission barriers has degraded between UNEDF0 (3 different types of nuclear data included in the optimization for a total of 108 data points) and UNEDF2 (5 data types, 130 points), while the ability to predict binding energies near closed shells and single-particle states increased. Note that until now, no attempt has been made to rigorously quantify the bias of EDF parameterizations.

The pairing channel represents an additional difficulty when determining the parameters of the nuclear EDF. Indeed, very little data can effectively and unambiguously constrain the pairing functional directly at the HFB level. In practice, the odd-even staggering (OES) of binding energies is most often used [67–71]. The UNEDF functionals were the first ones where the fit of the pairing functional was performed simultaneously with the fit of the Skyrme EDF. As a result, there are built-in correlations between the parameters of the Skyrme EDF and the two parameters that control the pairing functional.

3.1.2 Optimization algorithm

The minimization of the χ^2 function in the context of nuclear DFT remains costly in computational resources. In the example of the UNEDF functionals, 100+ full, HFB calculations in axially deformed nuclei must be performed in order to define the χ^2. Some of the most popular parameterizations of the nuclear EDF were published in the 1980s and 1990s, where the cost of running a full HFB calculation was prohibitive in terms of χ^2 minimization. Even now, the optimization of HFB mass models by the Bruxelles-Montréal Collaboration, where the χ^2 includes over 2500 points, is still performed with a DFT solver with built-in spherical symmetry. The effect of deformation in the ground-state binding energy is taken into account by using an empirical renormalization procedure; see [72] for details.

In view of this computational cost, specifically designed algorithms with a focus on efficiency and robustness are especially valuable. We recall that derivatives $\partial\eta_{ti}(\boldsymbol{x})/\partial x_\mu$ are not available analytically for the minimization of the χ^2 (9). Of course they can always be computed numerically, but at a significant cost when n_x is large. Therefore, the optimization of the nuclear EDF is most efficiently performed with derivative-free approaches.

Although a rich literature on the subject exists, we mention here only the Practical Optimization Using No Derivatives for sums of Squares (POUNDERS) algorithm developed in the framework of the UNEDF Collaboration [31, 73–75]. POUNDERS is a derivative-free trust-region method based on forming a local quadratic model of each component of the χ^2. The quadratic models are valid only in a small region of the parameter space near the current point $\boldsymbol{x}$, but their aggregate approximation can be minimized analytically. The minimum $\boldsymbol{x} + \delta\boldsymbol{x}$ defines the next point of a Newton-like procedure. As seen in fig. 2, the POUNDERS algorithm converges quickly compared to the traditional Nelder-Mead algorithm; most important, it gives a better solution. POUNDERS has

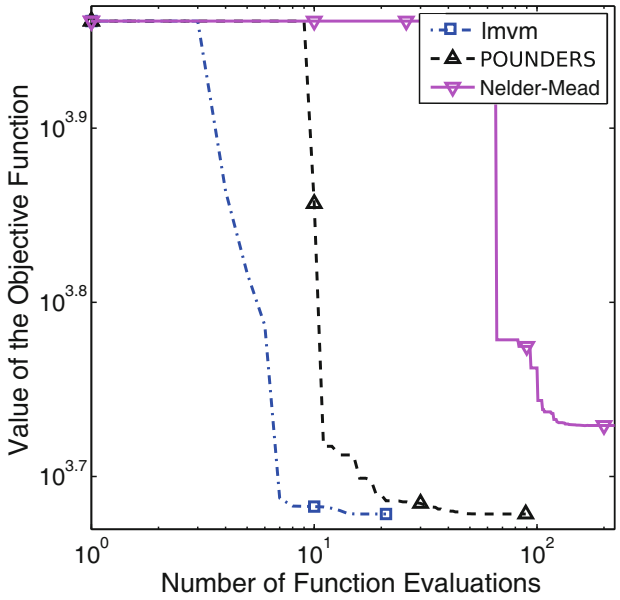

Fig. 2. Performance (log-log scale) of three solvers (limited-memory variable metric, POUNDERS Nelder-Mead) for nonlinear generalized χ^2 problems with $n_x = 6$ parameters and $n_d = 428$ data points; from [73].

Table 1. Root-mean-square deviations for each type of nuclear data included in the UNEDF1 χ^2 as a function of the standard deviation $\sigma_{\rm OES}$ used for OES data of both protons and neutrons; see text for details. All r.m.s. values are in MeV except the ones for proton radii, which are in fm; from [79].

$\sigma_{\rm OES}$	0.025	0.050	0.075	0.100
Deformed masses	0.944	0.776	2.596	0.806
Spherical masses	2.427	1.836	2.669	1.718
Proton radii	0.022	0.022	0.022	0.022
OES neutrons	0.012	0.051	0.065	0.080
OES protons	0.043	0.074	0.075	0.072
Fission isomer	0.809	0.558	0.535	0.530

recently been applied to other problems of interest in nuclear physics [76,77].

3.1.3 Choice of the objective function

Given a set of data points and a minimization algorithm, some latitude remains in defining the weights, or standard deviations σ_t, associated with each data type. These quantities represent the estimated error on the data type t. They are in principle determined in such a way that the χ^2 objective function (9) approaches 1 at the minimum. Satisfying this condition may require readjusting the weights during the minimization [78]. In practice, this step has rarely been done in nuclear EDF optimization, and the weights are most often kept constant (though data type dependent). In table 1, we show the impact of changing a single weight in the χ^2 objective function. In practice, we performed a refit of the UNEDF1 functional at the HFB approximation only. In the case of UNEDF1, the χ^2 function (9) is characterized by 4 different data types: masses in spherical (28 points) and deformed nuclei (47), proton radii in spherical nuclei (28), odd-even staggering in deformed nuclei (4 for protons, 4 for neutrons) and excitation energy of fission isomers actinide nuclei (4) [31]. This χ^2 function is the same for each column in table 1, with one exception: the weight of the OES data for both protons and neutron, which we vary between 0.025 MeV and 0.100 MeV (our reference result has $\sigma_{\rm OES} = 0.05$ MeV). In all cases, the minimization of the χ^2 is performed with the same algorithm, the same initial point, the same DFT solver, etc. We see that this single weight has a significant impact on the results, even if OES data accounts for no more than 8 out of the 115 data points included in the χ^2 (7% of the data set).

Minimizing the χ^2 (9) requires initializing the optimization algorithm with a vector $\boldsymbol{x}_0$. Ideally, the optimization algorithm would be able to converge to the absolute minimum of the objective function, given a set of constraints dictated by reality. In practice, it is nearly impossible to guarantee such a result. To our knowledge, there is only one example where the impact of the initial point on the resulting parameterization was studied in detail [73]. Table 2 illustrates the robustness of the

Table 2. Rerun of POUNDERS on the UNEDF0 problem ($n_d = 108$) from two different starting points: the SLy4 parametrization of the Skyrme EDF [80], and the SkM* parametrization [64]. The Skyrme EDF is characterized by the following parameters: ρ_c (saturation density) is in fm^{-3}; E^{NM}/A (binding energy per nucleon in nuclear matter), K^{NM} (incompressibility), $a_{\rm sym}^{NM}$ (symmetry energy coefficient), and $L_{\rm sym}^{NM}$ (slope of the symmetry energy) are in MeV; M_s^* (scalar effective mass) is dimensionless; $C_t^{\rho\Delta\rho}$ (surface coupling constants) and $C_t^{\rho\nabla J}$ (spin-orbit coupling constants), $t = 0, 1$ are in MeV fm^5; and V_0^n and V_0^p (pairing strengths) are in MeV fm^3. The column marked "final" shows the result of the optimization; bold face highlights identical digits; underlined values indicate that the corresponding parameters reached the boundary of their interval of variation during optimization and were frozen there.

	Starting from SLy4		**Starting from SKM***	
	SLy4	final	SkM*	final
ρ_c	0.159539	**0.160**486	0.160319	**0.160**435
E^{NM}/A	−15.9721	**−16.0**685	−16	**−16.0**73
K^{NM}	229.901	**230**	216.658	**230**
$a_{\rm sym}^{NM}$	32.0043	**31**.3393	30.0324	**31**.7221
$L_{\rm sym}^{NM}$	45.9618	54.2493	45.7704	60.4725
$1/M_s^*$	1.43955	**0.9**	1.26826	**0.9**
$C_0^{\rho\Delta\rho}$	−76.9962	**−55.2**344	−68.2031	**−55**.7348
$C_1^{\rho\Delta\rho}$	15.6571	−64.1619	17.1094	−70.4274
V_0^n	−285.84	**−170**.796	−280	**−170**.788
V_0^p	−285.84	**−197**.782	−280	**−198**.038
$C_0^{\rho\nabla J}$	−92.25	**−77**.9436	−97.5	**−79**.2915
$C_1^{\rho\nabla J}$	−30.75	27.4519	−32.5	**49**.5737
$f(\hat{\boldsymbol{x}})$	1188.75	**67**.9034	24814.1	**67**.5738

POUNDERS algorithm; similar solutions to the optimization problem are obtained when starting from the SLy4 or SkM* parameterization. The largest difference occurs for $L_{\rm sym}^{NM}$ (slope of the symmetry energy in nuclear matter at saturation density) and $C_1^{\rho\nabla J}$ (isovector spin-orbit coupling constant), which are poorly constrained by the data set [31].

3.2 Statistical uncertainties of energy densities

Irrespective of the form of the energy functional, the degree of arbitrariness in defining the χ^2 used to determine the "best" parameters of the EDF clearly suggests possibly large uncertainties in the resulting parameterizations. Standard methods of probability and statistics can be used to quantify some of these uncertainties. In this section, we review only the techniques used to estimate statistical uncertainties. Few studies of systematic uncertainties have been conducted so far; see [79] for discussion. Numerical errors are discussed separately in sect. 3.3. This separation is made for convenience only, since it is illusory to think that all sources of uncertainties can be completely disentangled.

3.2.1 Covariance analysis

One of the most common quantities used for estimating statistical uncertainties is the covariance matrix. The use of covariance techniques in nuclear DFT is relatively recent. Full regression analysis was first introduced in the context of nuclear mass fits in [81]. The covariance matrix was first mentioned and computed for Skyrme EDF optimization in [63]. Since then, there have been many applications of this technique to compute the standard deviation of EDF parameters and propagate uncertainties in model predictions; see sect. 4.

In the following, we denote $\boldsymbol{C}_M$ the covariance matrix of the parameters $\boldsymbol{x}$ of the model M that we are using (EDF), formally,

$$(C_M)_{ij} = E\left[(x_i - E(x_i))(x_j - E(x_j))\right], \qquad (10)$$

where $E()$ refers to the average of a random variable; each parameter x_i is thus treated as a random variable. One should distinguish $\boldsymbol{C}_M$ from the "data" covariance matrix $\boldsymbol{C}_D$. The latter notation will be used to refer to the covariance matrix of the random variables $\boldsymbol{\epsilon}$ associated with the error between the model output $\boldsymbol{\eta}(\boldsymbol{x})$ and the experimental data $\boldsymbol{y}$. All these misfits ϵ_{ti} are often assumed to be independent, therefore $\boldsymbol{C}_D$ is diagonal and $(C_D)_{ij} = \sigma_i^2\delta_{ij}$. One also assumes that they follow a (multivariate) normal distribution with mean 0, $\boldsymbol{\epsilon} \sim \mathcal{N}(0, \boldsymbol{C}_D)$.

In the simple case of an unweighted, linear least-squares optimization, where $\boldsymbol{\eta}(\boldsymbol{x}) = \boldsymbol{A}\boldsymbol{x}$ and $\sigma_i^2 = 1$, the inverse of the covariance matrix $\boldsymbol{C}_M$ can be computed as [60,61]

$$(C_M^{-1})_{ij}(\boldsymbol{x}) = \left(\frac{1}{2}\frac{\partial^2\chi^2}{\partial x_i \partial x_j}\right)^{-1} = 2\left(\mathcal{H}^{-1}\right)_{ij}, \qquad (11)$$

where $\mathcal{H}$ is the Hessian matrix of $(n_d - n_x)\chi^2(\boldsymbol{x})$. In the case of nuclear EDF optimization, the quality of the covariance matrix estimation is thus contingent on the linear dependence of observables with model parameters within the range of variation of interest. From the literature, one finds that nuclear binding energies behave linearly across a broad range of parameter space [79]; single-particle orbitals have a small degree of nonlinearity [82]; nonlinearities are more pronounced in the variation of fission isomer excitation energies [79]. While covariance techniques have been often employed recently to obtain estimates of statistical uncertainties on model predictions, see sect. 4, the underlying hypothesis of linearity has rarely been investigated in detail.

The covariance matrix can also be used to get an estimate of confidence intervals/regions. Recall that if the errors $\boldsymbol{\epsilon}$ follow a multivariate normal distribution, then the confidence interval at $\alpha \times 100$ percent for parameter i is defined by the endpoints

$$\hat{x}_i \pm \sqrt{(C_M)_{ii}}\, t_{n_d - n_x, 1-\frac{\alpha}{2}}, \qquad (12)$$

where $t_{n_d-n_x,1-\frac{\alpha}{2}}$ is the $1-\frac{\alpha}{2}$ quantile of the (Student's) t distribution with $n_d - n_x$ degrees of freedom [60,81,83–85]. This was used, for example, in the assessment of the UNEDF functionals [31–33]. The diagonal elements of the covariance matrix define the standard deviations, $(C_M)_{ii}$, of each parameter i.

3.2.2 Bayesian techniques

Bayesian inference techniques have been used for many years in the nuclear data community [86–90]. In nuclear structure, this method has recently gained ground, for example, to quantify uncertainties in chiral effective potentials [91,92]. In DFT, Bayesian inference has been used in electronic structure theory to evaluate errors in atomization and cohesive energies caused by the uncertainties in determining the exchange-correlation functional in the generalized gradient approximation [93].

Following [86], one may describe Bayesian techniques as an exercise of inductive inference when the probability for an hypothesis A to be true is interpreted not strictly as the number of observations of A over the total number of outcomes, but rather as the degree of plausibility that A is true. The "philosophical" interpretation is that the true value of the model parameters $\boldsymbol{x}$ is described probabilistically. Additional data further constrain the probability distribution but never reduces it to a single, known value.

Bayes' theorem provides the mathematical foundation for Bayesian techniques. In the case of continuous random variables, it reads

$$p(\boldsymbol{x}|\boldsymbol{y}, M)\mathrm{d}\boldsymbol{x} = \frac{P(\boldsymbol{y}|\boldsymbol{x}, M)P(\boldsymbol{x}|M)\mathrm{d}\boldsymbol{x}}{\displaystyle\int P(\boldsymbol{y}|M)\mathrm{d}\boldsymbol{x}}. \qquad (13)$$

In practice, we seek the probability $p(\boldsymbol{x}|\boldsymbol{y}, M)\mathrm{d}\boldsymbol{x}$ of the model M having parameters $\boldsymbol{x}$ based on a set of observed

data $\boldsymbol{y}$. The model is typically characterized by a number of features that add to the resulting uncertainties. In the case of EDF optimization, these features include the type of functional (Skyrme, Gogny, or other), the treatment of pairing correlations (HFB approximation, particle number projection), and the numerical implementation. The probability distribution $p(\boldsymbol{x}|\boldsymbol{y}, M)$ is the *posterior* distribution. Note that the posterior is computed within the model M: it does not contain any information about the validity of said model. In other words, suppose the posterior distribution is sharply peaked around a given value $\boldsymbol{x}_0$: the fact that $\boldsymbol{x}_0$ is the most likely parameter set does not mean i) that it is the correct one (since more data may change the distribution), and ii) that the resulting model is the correct one (since everything is model-dependent).

In eq. (13), $P(\boldsymbol{y}|\boldsymbol{x}, M)$ is the probability that the model produces the data given the parameters: it is the likelihood function [60]. $P(\boldsymbol{x}|M)$ is the probability that the model has parameters $\boldsymbol{x}$ irrespective of any data: it is the *prior* distribution. For a uniform prior distribution, maximizing the posterior distribution is equivalent to maximizing the likelihood. We remark in passing that both statistical approaches give different results if one looks at the probability distribution of some new parameter $g(\boldsymbol{x})$ that is a function of the original parameters $\boldsymbol{x}$ [60].

Bayesian inference can also be used to compute an estimate of the covariance matrix C_M between the parameters. Assuming weak nonlinearities of the model parameters, that is, $\boldsymbol{\eta}(\boldsymbol{x}) \propto \boldsymbol{x}$, the likelihood function is approximately Gaussian with respect to $\boldsymbol{x}$. If one assumes, for simplicity, full ignorance about the prior distribution (uniform distribution with independent parameters), then the posterior covariance matrix is given by [94]

$$\tilde{\boldsymbol{C}}_M^{-1} \approx \boldsymbol{G}^T \boldsymbol{C}_D^{-1} \boldsymbol{G}, \tag{14}$$

where

$$G_{ij}(\boldsymbol{x}) = \frac{\partial \eta_i}{\partial x_j}(\boldsymbol{x}) \tag{15}$$

and $\boldsymbol{C}_D$ is, as before, the covariance matrix associated with the misfits between data and the predictions. Owing to the (near) linearity of the model parameters, one can easily find that $\tilde{\boldsymbol{C}}_M^{-1} = 2\boldsymbol{\mathcal{H}}$ as obtained from the standard covariance matrix. The advantage of the Bayesian approach is the possiblity of including in the calculation of the covariance matrix the effect of prior knowledge of the distribution of model parameters; see sect. 3.2.3 in [94] for details.

Posterior distributions are typically sampled by using Markov chain Monte Carlo (MCMC) techniques [95], the result being a (dependent) sequence of samples $\{\boldsymbol{x}^{(1)}, \ldots, \boldsymbol{x}^{(T)}\}$. In practice, this sampling can be computationally challenging, since thousands or millions of evaluations of the likelihood function, hence of the χ^2 function, may be needed. As mentioned in sect. 3.1.2, the χ^2 functions used in nuclear EDF optimizations may typically involve between 100 and 2500 HFB calculations or more, making the direct sampling of the posterior distribution prohibitive. The alternative is to estimate response surface functions in order to emulate the behavior of the model response $\eta_{ti}(\boldsymbol{x})$ at a much cheaper cost [96–98]. The parameters of these response functions can also be incorporated in the statistical setting $\boldsymbol{x}$.

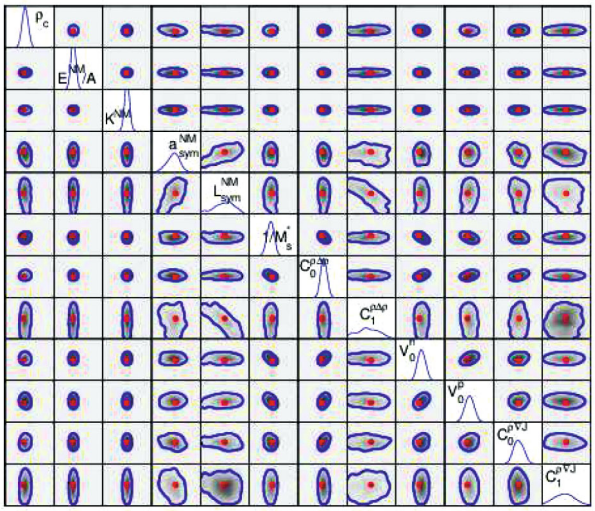

Fig. 3. Univariate and bivariate marginal estimates of the posterior distribution for the 12-dimensional DFT parameter vector of the UNEDF1 parameterization; see text for details. The blue lines enclose an estimated 95% confidence level region for the posterior distribution found when only the deformed masses from the original UNEDF1 data are accounted for. The red dot corresponds to the UNEDF1 values. The range of variation of each parameter i is $[\hat{x}_i - 3\sigma_i, \hat{x}_i + 3\sigma_i]$, with $\hat{x}_i$ the UNEDF1 value of the parameter, and σ_i it standard deviation; see [99] for additional details and table II in [32] for the values of $\hat{x}_i$ and σ_i.

Until now, there have been only two examples of Bayesian applications in nuclear EDF optimization. In [100], the backward-forward Monte-Carlo method was applied to estimate uncertainties in Skyrme mass model parameters. In [101], the full 12-dimensional multivariate posterior distribution of the Skyrme EDF corresponding to the UNEDF1 χ^2 was computed by using response functions based on Gaussian processes. The resulting univariate and bivariate marginal distributions are shown in fig. 3: the univariate distribution for parameter x_k is obtained by fixing all $x_{i\neq k}$ to their central, UNEDF1 values (represented by the red dots in the figure). Similarly, the bivariate marginal distribution for a pair of parameters (x_k, x_l) is obtained by fixing all other parameters $x_{i\neq k,l}$ to their central values. The characteristics of the posterior distribution, such as the calculated standard deviations of the parameters, are similar to the results from the analysis based on the confidence interval given in [32].

3.3 Numerical implementations

Implementing the DFT equation (*e.g.*, the HFB equations for the SR-EDF approach) in a computer program introduces numerical errors. These errors are unavoidable because the density matrix and pairing tensor have an infinite number of degrees of freedom. In this section, we focus

only on the problem of solving the HFB equations: in the SR-EDF approach, these are the only equations needed. In multireference EDF, the HFB equations also play a central role because errors in the solutions will propagate to the calculation of beyond mean-field corrections such as in the generator coordinate method [15].

One of the most popular approaches for solving the HFB equations is to expand the HFB solutions on a basis of known functions. In atomic nuclei, the eigenstates of the harmonic oscillator (HO) are most often used, since they are given analytically on spherical, cylindrical, and Cartesian coordinates. In addition, there is an exact separation between center of mass and relative motion, and the nuclear mean field is well approximated by an HO. Several DFT solvers using HO basis expansions have been published; see [8,22,51,102–108]. In practice, all basis expansions are truncated. Therefore, HFB solutions become dependent on the characteristic parameters of the basis; in the case of the HO, these are the basis frequencies $\boldsymbol{\omega} = (\omega_x, \omega_y, \omega_z)$, number of oscillator shells N, and total number of basis states (if the basis is spherical, all frequencies are identical and the number of states can be computed from the number of shells). This spurious dependence on the basis parameters may induce large errors, for example in nuclei with large elongations or weakly bound systems [79,109].

The HFB equations can also be solved by direct numerical integration; see, for example, [111] for the HFB formalism in coordinate space. This has been done in spherical and axial symmetry only [110,112]. In these two cases, the high precision of the coordinate space approach can be used to estimate the truncation error of HO expansion techniques. In the most recent DFT calculations of ground-state nuclear properties, up to 20 full oscillator shells are included in the basis [2]. Based on the results shown in fig. 4, this indicates that the absolute error on the binding energy would be at least of the order of 300 keV. If one wanted to reduce this error to less than 100 eV, up to $N = 60$ full oscillator shells should be included. This implies that the size of the U and V matrices of the Bogoliubov transformation would be of the order of 40000×40000, since the total number of states in the HO basis with N shells is $(N+1)(N+2)(N+3)/6$ [113]. In the case of fig. 4, spherical symmetry is assumed: one can take advantage of the degeneracy of single-particle states to make the U and V matrices block diagonal [28] and reduce the maximum block size to less than 2000×2000. In the general case of a nucleus with triaxial deformation, however, such block reduction is not possible and the cost of solving iteratively the HFB equations as described in sect. 2.1 becomes impractical unless the basis is significantly smaller.

For more complex geometries, the computational cost of direct numerical integration also becomes prohibitive; and hybrid strategies such as lattice discretization [114,115], finite element analysis [116,117] and multi-resolution wavelet expansion [118] have been investigated. In spite of their high precision, all of these techniques are computationally expensive in terms of processes, memory, or disk space. They are also not ideal for handling finite-range local forces or nonlocal forces.

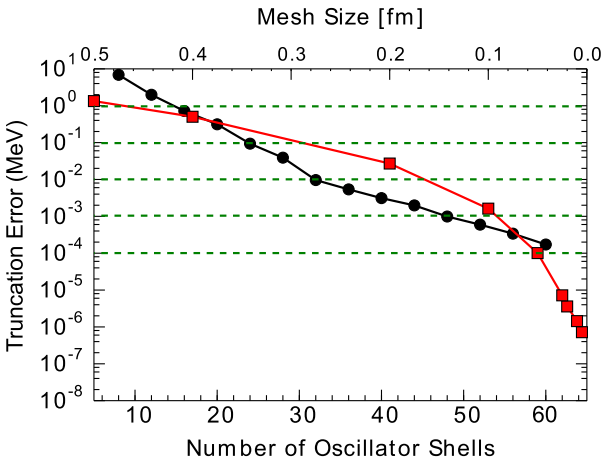

Fig. 4. Comparison between the pace of convergence of a spherical DFT calculation in coordinate-space, (red squares), and configuration space (HO basis), (black circles) for the ground state of ^{208}Pb. Results were obtained by setting both direct and exchange terms of the Coulomb potentials to 0. The HO basis results are optimized with respect to the oscillator frequency. Coordinate space calculations were performed with HFBRAD in a box of 20 fm [110], HO calculations with HOSPHE [8]. Dashed lines indicate truncation errors of 1 MeV, 100 keV, 10 keV, 1 keV and 100 eV; from [79].

Numerical errors inherent in DFT solvers are often overlooked, even though they may play a nonnegligible role in the estimation of statistical uncertainties. For example, the truncation error of HO expansions increases with nuclear deformation, even when one tries to adjust the geometry of the HO basis accordingly [109,119]. As a result, the numerical error in the energy of, say, the fission isomer or the top of the fission barriers in actinide nuclei is always going to be larger than the error in the ground state. In fact, at very large deformations, the error of one-center basis expansions can reach a few MeV. Apart from adopting empirical corrections based on auxiliary large-scale surveys of numerical errors [120], the solution could be to generalize asymptotic formulas such as proposed in the context of ab initio theory [121–123]. This problem, as well as the inclusion of these errors in the calculation of uncertainties, remains open.

4 Uncertainty propagation and predictive power

One of the main advantages of using the statistical analysis techniques briefly presented in sect. 3 is to provide a rigorous framework for propagating the quantified uncertainties to predictions. These predictions can be the result of running the same model on a different data set; for example, computing masses of exotic neutron-rich nuclei or superheavy elements that have not been included in the data set during the optimization [101].

Most important, uncertainties in the EDF could also, in principle, be propagated to cases where the EDF is only one of several theoretical components, each with a few

sources of uncertainties. The calculation of low-lying excited states within the quasiparticle random phase approximation (QRPA) is a straightforward example: it typically contains approximation of its own (symmetry restrictions, limited model space, etc.), but it is also strongly dependent on the EDF.

Let us firmly reassert here that in both cases, propagating uncertainties estimated using covariance of Bayesian techniques provides information only about the impact of said uncertainties. The procedure does little to provide ways to reduce them. In EDF optimization, numerical errors due to basis or mesh truncation can easily (at least in principle) be remedied. Statistical and *a fortiori* systematic uncertainties are much more difficult to address without a detailed understanding of the nuclear many-body problem.

Most uncertainty propagation reported in the literature was performed with covariance techniques. This situation implies that computed observables are linearly dependent on model parameters, which is guaranteed only locally near the optimal point. The computed value $\eta_y(\boldsymbol{x})$ of a single new observable y depends on the parameterization of the EDF, and one can estimate its standard deviation based on the parameter covariance matrix $\boldsymbol{C}_M$ [60,94]:

$$\sigma_y^2 = \sum_{ij} G_{yi}(\boldsymbol{C}_M^{-1})_{ij} G_{yj}, \qquad G_{yi}(\boldsymbol{x}) = \frac{\partial \eta_y}{\partial x_i}(\boldsymbol{x}). \quad (16)$$

If one now considers two new observables y and y', possibly correlated, such as the neutron skin in ^{208}Pb and electric dipole (E1) polarizability α_D in the same nucleus, then the above formula should be generalized to

$$\boldsymbol{C}_{yy'} = \boldsymbol{G}^T \boldsymbol{C}_M^{-1} \boldsymbol{G} \quad (17)$$

to account for cross-correlations.

In the context of DFT applications, such covariance analysis has been applied to compare statistical and systematic uncertainties of neutron skins [124]; to explore the properties of ground-state properties of closed-shell nuclei far from stability [125]; and to optimize EDF for nuclear astrophysics [126–128].

Bayesian techniques have been introduced only recently in nuclear theory in general, and EDF optimization in particular. As a result, in only a couple of cases have these methods been applied to the propagation of uncertainties. In [100], the backward-forward Monte-Carlo algorithm [129], which is a particular implementation of Bayesian inference, was used to estimate the statistical uncertainties in Skyrme mass models. In [79,101], the full posterior distribution of the UNEDF1 Skyrme EDF was determined in a statistical setting by using Bayesian inference, with uniform prior for $\boldsymbol{x}$ and a Gaussian process to emulate the response of the model $\eta(\boldsymbol{x})$. The posterior distribution was then sampled and used to estimate uncertainties on the fission barrier of ^{240}Pu and the position of the two-neutron dripline. The large uncertainties on fission barriers visible in fig. 5 emphasizes the lack of constraints on model parameters, which could be caused by an inappropriate choice of experimental data and/or too limited a model (in this case the Skyrme EDF).

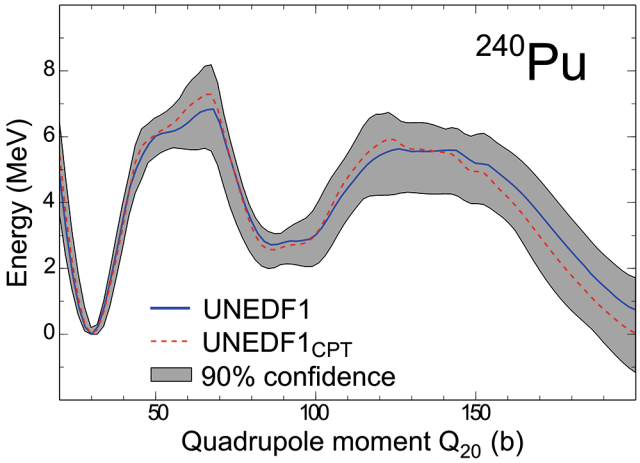

Fig. 5. Comparison between the fission barrier predictions for ^{240}Pu made with the original UNEDF1 (solid line), with a refit of UNEDF1 including 17 more masses in neutron-rich nuclei measured in the Canadian Penning Trap (CPT) at Argonne National Laboratory (dashed line), together with the 90% confidence interval (shaded gray area) obtained from the Bayesian analysis of the original UNEDF1; from [101].

In addition to the applications mentioned in the previous section, a few attempts have been made to propagate statistical uncertainties from the nuclear EDF to the calculation of observables that involve another model. For example, quantifying the impact of neutron skins on the electric dipole polarizability or on the weak-charge form factor requires calculating the electric dipole response function, that is, RPA calculations [130–132].

5 Conclusions

Over the past decade, nuclear density functional theory has positioned itself as a candidate for a global, comprehensive, accurate, and predictive theory of nuclear structure. Thanks to the (very recent) introduction in this field of standard statistical tools such as covariance techniques or Bayesian inference, the statistical uncertainties associated with the most common energy functionals such as the Skyrme, Gogny, or relativistic EDF have been computed rigorously. The propagation of these uncertainties to model predictions in nuclei far from stability has often highlighted the need to substantially improve the constraints on the parameters of the nuclear EDF, irrespective of the origin of the functional itself. Progress is thus needed in two complementary directions. Better rooting of the nuclear EDF in the theory of nuclear forces will provide much-needed constraints on the expected predictive power of the theory. This effort should go hand in hand with the generalization of statistical techniques to the problem of EDF optimization, and the always-indispensable conversations with the experimental nuclear physics and data communities.

On a practical level, an exciting avenue of research would be to extend the use of statistical techniques to

complex problems where the nuclear EDF is one of several theoretical tools used. For example, properties of the neutron spectrum in neutron-induced fission are currently described within the Hauser-Feshbach approach to nuclear reactions. Such calculations require fission fragment yields, total kinetic energies, and excitation energies of the fragments. These quantities, in turn, are currently obtained from either semi-phenomenological models based, for example, on Langevin dynamics [133,134], or from fully microscopic calculations based on the time-dependent generator coordinate method [135–137]. Either way, these dynamical calculations depend on the potential energy surface of the nucleus in some pre-defined collective space. For the microscopic approach, this potential energy surface depends on which nuclear EDF is used, how the EDF has been fitted, and what types of corrections are included [32,138–142]. Ultimately, one would therefore wish to propagate the uncertainties all the way through this chain of "models," from the nuclear EDF to the fission spectrum.

A related area of future research would be to define a comprehensive framework to address uncertainties. In this manuscript, we have insisted on the statistical uncertainties, with only a short discussion of numerical errors. However, we have also pointed out that all forms of uncertainties are related to one another: numerical errors are not a constant offset in DFT calculations, and thus they propagate in a very nonlinear way into the calculation of the χ^2, which will impact parameter optimization and subsequent uncertainty analysis. The particular mathematical formulation of the theory (SR-EDF versus MR-EDF, HFB approximation only or HFB plus corrections, etc.) also partially determines which observables can be reliably computed by the model. For all others, the statistical analysis may reveal that some parameters are ill-constrained, not because the data is insufficient, but because the model is not sensitive to it. Moreover, one should work toward incorporating experimental uncertainties. In the case of the UNEDF2 parameterization, for example, both fission isomer excitation energies and single-particle states were included in the fit. Yet these quantities are model-dependent, and their "experimental" error is rather large. In the future, one should try to incorporate this information in the determination of EDF parameters.

This material is based upon work supported by the U.S. Department of Energy, Office of Science, Office of Nuclear Physics under award numbers DE-AC52-07NA27344 (Lawrence Livermore National Laboratory), DE-AC02-06CH11357 (Argonne National Laboratory), and DE-SC0008511 (NUCLEI SciDAC Collaboration), and by the NNSA's Stewardship Science Academic Alliances Program under award no. DE-NA0001820. Computational resources were provided through an INCITE award "Computational Nuclear Structure" by the National Center for Computational Sciences and National Institute for Computational Sciences at Oak Ridge National Laboratory, through an award by the Livermore Computing Resource Center at Lawrence Livermore National Laboratory, and through an award by the Laboratory Computing Resource Center at Argonne National Laboratory.

References

1. Karl-Heinz Schmidt, Beatriz Jurado, Charlotte Amouroux, *General description of fission observables*, Technical Report NEA/DB/DOC(2014)1, Organisation for Economic Co-Operation and Development, Nuclear Energy Agency-OECD/NEA, Le Seine Saint-Germain, 12 boulevard des Iles, F-92130 Issy-les-Moulineaux (France) (2014).
2. Jochen Erler, Noah Birge, Markus Kortelainen, Witold Nazarewicz, Erik Olsen, Alexander M. Perhac, Mario Stoitsov, Nature **486**, 509 (2012).
3. Scott Bogner, Aurel Bulgac, J. Carlson, Jonathan Engel, George Fann, Richard J. Furnstahl, Stefano Gandolfi, Gaute Hagen, Mihai Horoi, C. Johnson, Comput. Phys. Commun. **184**, 2235 (2013).
4. S. Goriely, N. Chamel, J.M. Pearson, Phys. Rev. C **88**, 061302 (2013).
5. S. Goriely, S. Hilaire, M. Girod, S. Péru, Phys. Rev. Lett. **102**, 242501 (2009).
6. J.E. Drut, R.J. Furnstahl, L. Platter, Prog. Part. Nucl. Phys. **64**, 120 (2010).
7. M. Stoitsov, M. Kortelainen, S.K. Bogner, T. Duguet, R.J. Furnstahl, B. Gebremariam, N. Schunck, Phys. Rev. C **82**, 054307 (2010).
8. B.G. Carlsson, J. Dobaczewski, J. Toivanen, P. Veselý, Comput. Phys. Commun. **181**, 1641 (2010).
9. T. Duguet, J. Phys. G: Nucl. Part. Phys. **42**, 025107 (2015).
10. P. Hohenberg, W. Kohn, Phys. Rev. **136**, B864 (1964).
11. W. Kohn, L.J. Sham, Phys. Rev. **140**, A1133 (1965).
12. R.G. Parr, W. Yang, *Density Functional Theory of Atoms and Molecules* (Oxford University Press, Oxford, 1989).
13. R.M. Dreizler, E.K.U Gross, *Density Functional Theory: An Approach to the Quantum Many-Body Problem* (Springer-Verlag, 1990).
14. R. Eschrig, *Fundamentals of Density Functional Theory* (Teubner, Leipzig, 1996).
15. Michael Bender, Paul-Henri Heenen, Paul-Gerhard Reinhard, Rev. Mod. Phys. **75**, 121 (2003).
16. P. Ring, P. Schuck, *The Nuclear Many-Body Problem* (Springer-Verlag, 2000).
17. T. Duguet, *The nuclear energy density functional formalism*, in *The Euroschool on Exotic Beams, Vol. IV*, edited by Christoph Scheidenberger, Marek Pfützner, Vol. **879** (Springer Berlin Heidelberg, Berlin, Heidelberg, 2014) pp. 293–350.
18. J.-P. Blaizot, G. Ripka, *Quantum Theory of Finite Systems* (The MIT Press, Cambridge, 1985).
19. D.M. Brink, R.A. Broglia (Editors), *Nuclear Superfluidity – Pairing in Finite Systems* (Cambridge University Press, 2005).
20. J.G. Valatin, Phys. Rev. **122**, 1012 (1961).
21. Hans-Jörg Mang, Phys. Rep. **18**, 325 (1975).
22. J. Dobaczewski, J. Dudek, Comput. Phys. Commun. **131**, 164 (2000).
23. J. Dobaczewski, J. Dudek, S.G. Rohoziński, T.R. Werner, Phys. Rev. C **62**, 014310 (2000).
24. S.G. Rohoziński, J. Dobaczewski, W. Nazarewicz, Phys. Rev. C **81**, 014313 (2010).
25. Andrzej Baran, Aurel Bulgac, Michael Forbes, Gaute Hagen, Witold Nazarewicz, Nicolas Schunck, Mario Stoitsov, Phys. Rev. C **78**, 014318 (2008).

26. T.H.R. Skyrme, Nucl. Phys. **9**, 615 (1959).
27. D. Vautherin, D.M. Brink, Phys. Rev. C **5**, 626 (1972).
28. J. Dechargé, D. Gogny, Phys. Rev. C **21**, 1568 (1980).
29. J.R. Stone, P.-G. Reinhard, Prog. Part. Nucl. Phys. **58**, 587 (2007).
30. J. Erler, P. Klüpfel, P.-G. Reinhard, J. Phys. G: Nucl. Part. Phys. **37**, 064001 (2010).
31. M. Kortelainen, T. Lesinski, J. Moré, W. Nazarewicz, J. Sarich, N. Schunck, M.V. Stoitsov, S. Wild, Phys. Rev. C **82**, 024313 (2010).
32. M. Kortelainen, J. McDonnell, W. Nazarewicz, P.-G. Reinhard, J. Sarich, N. Schunck, M.V. Stoitsov, S.M. Wild, Phys. Rev. C **85**, 024304 (2012).
33. M. Kortelainen, J. McDonnell, W. Nazarewicz, E. Olsen, P.-G. Reinhard, J. Sarich, N. Schunck, S.M. Wild, D. Davesne, J. Erler, A. Pastore, Phys. Rev. C **89**, 054314 (2014).
34. M. Anguiano, J.L. Egido, L.M. Robledo, Nucl. Phys. A **683**, 227 (2001).
35. M.V. Stoitsov, J. Dobaczewski, R. Kirchner, W. Nazarewicz, J. Terasaki, Phys. Rev. C **76**, 014308 (2007).
36. M. Bender, K. Bennaceur, T. Duguet, P.-H. Heenen, T. Lesinski, J. Meyer, Phys. Rev. C **80**, 064302 (2009).
37. T. Duguet, T. Lesinski, *Non-Empirical Nuclear Energy Functionals, Pairing Gaps and Odd-Even Mass Differences* (AIP, 2009) p. 243.
38. D. Lacroix, T. Duguet, M. Bender, Phys. Rev. C **79**, 044318 (2009).
39. F. Raimondi, K. Bennaceur, J. Dobaczewski, J. Phys. G: Nucl. Part. Phys. **41**, 055112 (2014).
40. J. Sadoudi, T. Duguet, J. Meyer, M. Bender, Phys. Rev. C **88**, 064326 (2013).
41. J. Sadoudi, M. Bender, K. Bennaceur, D. Davesne, R. Jodon, T. Duguet, Phys. Scr. **T154**, 014013 (2013).
42. S.A. Fayans, S.V. Tolokonnikov, E.L. Trykov, D. Zawischa, Phys. Lett. B **338**, 1 (1994).
43. E. Krömer, S.V. Tolokonnikov, S.A. Fayans, D. Zawischa, Phys. Lett. B **363**, 12 (1995).
44. S.A. Fayans, S.V. Tolokonnikov, E.L. Trykov, D. Zawischa, Nucl. Phys. A **676**, 49 (2000).
45. M. Baldo, P. Schuck, X. Viñas, Phys. Lett. B **663**, 390 (2008).
46. M. Baldo, L.M. Robledo, P. Schuck, X. Viñas, Phys. Rev. C **87**, 064305 (2013).
47. Guillaume Hupin, Denis Lacroix, Phys. Rev. C **83**, 024317 (2011).
48. Guillaume Hupin, Denis Lacroix, Michael Bender, Phys. Rev. C **84**, 014309 (2011).
49. Guillaume Hupin, Denis Lacroix, Phys. Rev. C **86**, 024309 (2012).
50. Thomas Lesinski, Phys. Rev. C **89**, 044305 (2014).
51. Jacek Dobaczewski, J. Phys. G: Nucl. Part. Phys. **36**, 105105 (2009).
52. X.B. Wang, J. Dobaczewski, M. Kortelainen, L.F. Yu, M.V. Stoitsov, Phys. Rev. C **90**, 014312 (2014).
53. J. Engel, Phys. Rev. C **75**, 014306 (2007).
54. Jérémie Messud, Michael Bender, Eric Suraud, Phys. Rev. C **80**, 054314 (2009).
55. J. Dobaczewski, W. Nazarewicz, M.V. Stoitsov, *Contact pairing interaction for the Hartree-Fock-Bogoliubov calculations*, in *The Nuclear Many-Body Problem 2001* (Springer, 2002).
56. Yuan Tian, Zhong-yu Ma, Peter Ring, Phys. Rev. C **79**, 064301 (2009).
57. Yuan Tian, Zhong-yu Ma, P. Ring, Phys. Rev. C **80**, 024313 (2009).
58. S.K. Bogner, R.J. Furnstahl, H. Hergert, M. Kortelainen, P. Maris, M. Stoitsov, J.P. Vary, Phys. Rev. C **84**, 044306 (2011).
59. S. Gandolfi, J. Carlson, Steven C. Pieper, Phys. Rev. Lett. **106**, 012501 (2011).
60. W.J. Metzger, *Statistical methods in data analysis*, Technical report, Katholieke Universiteit Nijmegen (2002).
61. Siegmund Brandt, *Data Analysis - Statistical and Computational Methods for Scientists and Engineers* (Springer, 2014).
62. S. Goriely, M. Samyn, J. Pearson, Phys. Rev. C **75**, 064312 (2007).
63. P. Klüpfel, P.-G. Reinhard, T.J. Bürvenich, J.A. Maruhn, Phys. Rev. C **79**, 034310 (2009).
64. J. Bartel, Ph Quentin, Matthias Brack, C. Guet, H.-B. Håkansson, Nucl. Phys. A **386**, 79 (1982).
65. J.F. Berger, M. Girod, D. Gogny, Comput. Phys. Commun. **63**, 365 (1991).
66. G. Audi, A.H. Wapstra, C. Thibault, Nucl. Phys. A **729**, 337 (2003).
67. W. Satuła, J. Dobaczewski, W. Nazarewicz, Phys. Rev. Lett. **81**, 3599 (1998).
68. K. Rutz, M. Bender, P.-G. Reinhard, J.A. Maruhn, Phys. Lett. B **468**, 1 (1999).
69. J. Dobaczewski, W. Nazarewicz, P.-G. Reinhard, Nucl. Phys. A **693**, 361 (2001).
70. T. Duguet, P. Bonche, P.-H. Heenen, J. Meyer, Phys. Rev. C **65**, 014311 (2001).
71. G. Bertsch, C. Bertulani, W. Nazarewicz, N. Schunck, M. Stoitsov, Phys. Rev. C **79**, 034306 (2009).
72. F. Tondeur, S. Goriely, J.M. Pearson, M. Onsi, Phys. Rev. C **62**, 024308 (2000).
73. Stefan M. Wild, Jason Sarich, Nicolas Schunck, J. Phys. G: Nucl. Part. Phys. **42**, 034031 (2015).
74. T. Munson, J. Sarich, Stefan M. Wild, S. Benson, L. Curfman McInnes, *TAO 2.0 users manual*, Tech. Memo. ANL/MCS-TM-322, Argonne National Laboratory, Argonne, IL, 2012.
75. Stefan M. Wild, *Solving derivative-free nonlinear least squares with POUNDERS*, Preprint ANL/MCS-P5120-0414, Argonne, April 2014.
76. A. Ekström, G. Baardsen, C. Forssén, G. Hagen, M. Hjorth-Jensen, G.R. Jansen, R. Machleidt, W. Nazarewicz, T. Papenbrock, J. Sarich, S.M. Wild, Phys. Rev. Lett. **110**, 192502 (2013).
77. M. Bertolli, T. Papenbrock, S.M. Wild, Phys. Rev. C **85**, 014322 (2012).
78. J. Dobaczewski, W. Nazarewicz, P.-G. Reinhard, J. Phys. G: Nucl. Part. Phys. **41**, 074001 (2014).
79. N. Schunck, D. Duke, H. Carr, Phys. Rev. C **91**, 034327 (2015).
80. E. Chabanat, P. Bonche, P. Haensel, J. Meyer, R. Schaeffer, Nucl. Phys. A **627**, 710 (1997).
81. J. Toivanen, J. Dobaczewski, M. Kortelainen, K. Mizuyama, Phys. Rev. C **78**, 034306 (2008).
82. M. Kortelainen, J. Dobaczewski, K. Mizuyama, J. Toivanen, Phys. Rev. C **77**, 064307 (2008).

83. D.C. Montgomery, G.C. Runger (Editors), *Applied Statistics and Probability for Engineers* (John Wiley & Sons, Inc., 2002).
84. J. Dudek, B. Szpak, M.-G. Porquet, B. Fornal, J. Phys.: Conf. Ser. **267**, 012062 (2011).
85. B. Szpak, J. Dudek, M.-G. Porquet, B. Fornal, J. Phys.: Conf. Ser. **267**, 012063 (2011).
86. F.H. Fröhner, *Evaluation and analysis of nuclear resonance data*, Technical Report 18, OECD Nuclear Energy Agency, Paris, 2000.
87. H. Leeb, D. Neudecker, Th. Srdinko, Nucl. Data Sheets **109**, 2762 (2008).
88. Roberto Capote, Donald L. Smith, Nucl. Data Sheets **109**, 2768 (2008).
89. M. Herman, A. Koning, *Covariance data in the fast neutron region.* Technical Report 24, Technical report NEA/WPEC-24, OECD Nuclear Energy Agency, Paris, 2011.
90. Patrick Talou, Toshihiko Kawano, Mark B. Chadwick, Denise Neudecker, Michael E. Rising, J. Phys. G: Nucl. Part. Phys. **42**, 034025 (2015).
91. M.R. Schindler, D.R. Phillips, Ann. Phys. **324**, 682 (2009).
92. R.J. Furnstahl, D.R. Phillips, S. Wesolowski, J. Phys. G: Nucl. Part. Phys. **42**, 034028 (2015).
93. J.J. Mortensen, K. Kaasbjerg, S.L. Frederiksen, J.K. Nørskov, J.P. Sethna, K.W. Jacobsen, Phys. Rev. Lett. **95**, 216401 (2005).
94. Albert Tarantola, *Inverse problem theory and methods for model parameter estimation* (Society for Industrial and Applied Mathematics, Philadelphia, 2005).
95. D. Gamerman, H.F. Lopes, *Markov Chain Monte Carlo: Stochastic Simulation for Bayesian Inference* (Chapman & Hall/CRC, 2006).
96. Marc C. Kennedy, Anthony O'Hagan, J. R. Stat. Soc. **63**, 425 (2001).
97. Dave Higdon, James Gattiker, Brian Williams, Maria Rightley, J. Am. Stat. Assoc. **103**, 570 (2008).
98. Ilias Bilionis, Nicholas Zabaras, Bledar A. Konomi, Guang Lin, J. Comput. Phys. **241**, 212 (2013).
99. Nicolas Schunck, Jordan D. McDonnell, Jason Sarich, Stefan M. Wild, Dave Higdon, J. Phys. G: Nucl. Part. Phys. **42**, 034024 (2015).
100. S. Goriely, R. Capote, Phys. Rev. C **89**, 054318 (2014).
101. J.D. McDonnell, N. Schunck, D. Higdon, J. Sarich, S.M. Wild, W. Nazarewicz, Phys. Rev. Lett. **114**, 122501 (2015).
102. J. Dobaczewski, J. Dudek, Comput. Phys. Commun. **102**, 166 (1997).
103. J. Dobaczewski, J. Dudek, Comput. Phys. Commun. **102**, 183 (1997).
104. J. Dobaczewski, P. Olbratowski, Comput. Phys. Commun. **158**, 158 (2004).
105. J. Dobaczewski, P. Olbratowski, Comput. Phys. Commun. **167**, 214 (2005).
106. M.V. Stoitsov, J. Dobaczewski, W. Nazarewicz, P. Ring, Comput. Phys. Commun. **167**, 43 (2005).
107. N. Schunck, J. Dobaczewski, J. McDonnell, W. Satuła, J.A. Sheikh, A. Staszczak, M. Stoitsov, P. Toivanen, Comput. Phys. Commun. **183**, 166 (2012).
108. M.V. Stoitsov, N. Schunck, M. Kortelainen, N. Michel, H. Nam, E. Olsen, J. Sarich, S. Wild, Comput. Phys. Commun. **184**, 1592 (2013).
109. Nicolas Schunck, J. Phys.: Conf. Ser. **436**, 012058 (2013).
110. K. Bennaceur, J. Dobaczewski, Comput. Phys. Commun. **168**, 96 (2005).
111. J. Dobaczewski, H. Flocard, J. Treiner, Nucl. Phys. A **422**, 103 (1984).
112. J. Pei, M. Stoitsov, G. Fann, W. Nazarewicz, N. Schunck, F. Xu, Phys. Rev. C **78**, 064306 (2008).
113. A. Bohr, B.R. Mottelson, *Nuclear Structure*, Vol. **II** (Benjamin, New-York, 1975).
114. P. Bonche, H. Flocard, P.H. Heenen, Comput. Phys. Commun. **171**, 49 (2005).
115. W. Ryssens, V. Hellemans, M. Bender, P.-H. Heenen, Comput. Phys. Commun. **187**, 175 (2015).
116. W. Pöschl, D. Vretenar, A. Rummel, P. Ring, Comput. Phys. Commun. **101**, 75 (1997).
117. W. Pöschl, D. Vretenar, P. Ring, Comput. Phys. Commun. **103**, 217 (1997).
118. J.C. Pei, G.I. Fann, R.J. Harrison, W. Nazarewicz, Yue Shi, S. Thornton, Phys. Rev. C **90**, 024317 (2014).
119. M. Samyn, S. Goriely, J. Pearson, Phys. Rev. C **72**, 044316 (2005).
120. S. Hilaire, M. Girod, Eur. Phys. J. A **33**, 237 (2007).
121. S.A. Coon, M.I. Avetian, M.K.G. Kruse, U. van Kolck, P. Maris, J.P. Vary, Phys. Rev. C **86**, 054002 (2012).
122. R.J. Furnstahl, G. Hagen, T. Papenbrock, Phys. Rev. C **86**, 031301 (2012).
123. S.N. More, A. Ekström, R.J. Furnstahl, G. Hagen, T. Papenbrock, Phys. Rev. C **87**, 044326 (2013).
124. M. Kortelainen, J. Erler, W. Nazarewicz, N. Birge, Y. Gao, E. Olsen, Phys. Rev. C **88**, 031305 (2013).
125. Y. Gao, J. Dobaczewski, M. Kortelainen, J. Toivanen, D. Tarpanov, Phys. Rev. C **87**, 034324 (2013).
126. J. Erler, C.J. Horowitz, W. Nazarewicz, M. Rafalski, P.-G. Reinhard, Phys. Rev. C **87**, 044320 (2013).
127. N. Paar, Ch.C. Moustakidis, T. Marketin, D. Vretenar, G.A. Lalazissis, Phys. Rev. C **90**, 011304 (2014).
128. Wei-Chia Chen, J. Piekarewicz, Phys. Rev. C **90**, 044305 (2014).
129. E. Bauge, P. Dossantos-Uzarralde, J. Kor. Phys. Soc. **59**, 1218 (2011).
130. J. Piekarewicz, B.K. Agrawal, G. Colò, W. Nazarewicz, N. Paar, P.-G. Reinhard, X. Roca-Maza, D. Vretenar, Phys. Rev. C **85**, 041302 (2012).
131. P.-G. Reinhard, J. Piekarewicz, W. Nazarewicz, B.K. Agrawal, N. Paar, X. Roca-Maza, Phys. Rev. C **88**, 034325 (2013).
132. P.-G. Reinhard, W. Nazarewicz, Phys. Rev. C **87**, 014324 (2013).
133. Jørgen Randrup, Peter Möller, Phys. Rev. Lett. **106**, 132503 (2011).
134. J. Randrup, P. Möller, A.J. Sierk, Phys. Rev. C **84**, 034613 (2011).
135. H. Goutte, P. Casoli, J.-F. Berger, Nucl. Phys. A **734**, 217 (2004).
136. W. Younes, D. Gogny, *Collective dissipation from saddle to scission in a microscopic approach*, Technical Report LLNL-TR-586694, Lawrence Livermore National Laboratory (LLNL) Livermore, CA, 2012.
137. D. Regnier, M. Verrière, N. Dubray, N. Schunck, *FELIX-1.0: A finite element solver for the time dependent generator coordinate method with the Gaussian overlap approximation*, arXiv:1505.02704 (2015).

138. N. Nikolov, N. Schunck, W. Nazarewicz, M. Bender, J. Pei, Phys. Rev. C **83**, 034305 (2011).
139. T.V. Nhan Hao, P. Quentin, L. Bonneau, Phys. Rev. C **86**, 064307 (2012).
140. J.D. McDonnell, W. Nazarewicz, J.A. Sheikh, Phys. Rev. C **87**, 054327 (2013).
141. Samuel A. Giuliani, Luis M. Robledo, Phys. Rev. C **88**, 054325 (2013).
142. N. Schunck, D. Duke, H. Carr, A. Knoll, Phys. Rev. C **90**, 054305 (2014).